IEEE Access
Multidisciplinary ⋮ Rapid Review ⋮ Open Access Journal

Received May 24, 2020, accepted May 31, 2020, date of publication June 3, 2020, date of current version June 25, 2020.

Digital Object Identifier 10.1109/ACCESS.2020.2999659

Multi-Frequency Air-to-Ground Channel Measurements and Analysis for UAV Communication Systems

ZHUANGZHUANG CUI[1], (Graduate Student Member, IEEE), CÉSAR BRISO-RODRÍGUEZ[2], KE GUAN[1], (Senior Member, IEEE), ZHANGDUI ZHONG[1], (Senior Member, IEEE), AND FRANÇOIS QUITIN[3], (Member, IEEE)

[1]State Key Laboratory of Rail Traffic Control and Safety, Beijing Jiaotong University, Beijing 100044, China
[2]ETSIS Telecommunications, Technical University of Madrid, 28031 Madrid, Spain
[3]Brussels School of Engineering, Université Libre de Bruxelles, 1050 Brussels, Belgium

Corresponding author: Ke Guan (kguan@bjtu.edu.cn)

This work was supported in part by the NSFC under Grant 61771036, Grant 61911530260, and Grant 61901029, and in part by the State Key Laboratory of Rail Traffic Control and Safety under Contract RCS2019ZZ005.

ABSTRACT In order to implement unmanned aerial vehicle (UAV)-based wireless communications, a better understanding of wireless channels and the corresponding channel characterizations are critical. In this paper, air-to-ground (AG) channel measurements are carried out at some candidate frequencies, i.e., 1 GHz, 4 GHz, 12 GHz, and 24 GHz. With measurement data, the crucial channel parameters are comprehensively analyzed. Firstly, based on the channel model in the 3rd Generation Partnership Project (3GPP), the essential coefficients for modeling path loss, including path loss exponents (PLEs) and height-dependent factors, are obtained for AG channels. Then, a novel autocorrelation model for shadow fading is proposed. Besides, the small-scale fading is statistically analyzed, where the log-logistic distribution is found as the best fit among popular distributions. Moreover, the second-order statistical characteristics, including the level crossing rate (LCR) and average fade duration (AFD), are extracted to describe in-depth the fading behavior. Overall, the results and findings in this paper are essential for realizing reliable communications in AG wireless systems.

INDEX TERMS Air-to-ground (AG) channel, characterizations, fading behavior, measurements, UAV.

I. INTRODUCTION

Recently, unmanned aerial vehicle (UAV) has drawn much attention in wireless communications since it has been regarded as an essential enabler for realizing broad coverage and high-speed data rates [1]. For instance, thanks to its high flexibility in the deployment, the drone can be used as a temporary base station (BS) to provide communication services as an alternative or supplement of cellular systems in the disaster or hot-spot scenarios. Moreover, the cellular-connected UAV communication is also highlighted to perform long-distance on-demand tasks [2]. In this context, the corresponding drone-based air-to-ground (AG) channels are required to be characterized carefully and modeled accurately, since wireless channels are fundamental to the design and deployment of communication systems [3]. Meantime, a challengeable issue in AG channel modeling that needs to be focused on is the variety of candidate frequencies for UAV communication systems, since there is a vacancy of uniform regulation for the frequency usage. In terms of channel modeling, taking the frequency into considerations helps provide a more comprehensive model so that such a model has better generality and thus can be used in various scenarios with different operating frequencies.

Recent studies in AG channel modeling mainly focus on low-frequency bands, such as the bands of IEEE 802.11a/g (2.4 GHz, 5.8 GHz), or L-band (1-2 GHz), C-band (4-8 GHz) which are recommended for UAV communications by International Telecommunication Union (ITU) [4]. However, the higher frequency bands, such as K_u-band (12-18 GHz) and K-band (18-26.5 GHz) are rarely involved. It is well known that drones are also used in the middle

The associate editor coordinating the review of this manuscript and approving it for publication was Faissal El Bouanani.

layer of the space-air-ground integrated network (SAGIN), which needs to realize connections with ground terminals, as well as with satellites that generally work in the C-band, K_u-band, K-band [5]. It is acknowledged that the current cellular networks mainly work in the sub-6 GHz. However, given the potential applications in the beyond-6 GHz for the future SAGIN, the frequency bands we focus on in this paper include some representative bands in sub-6 GHz and beyond-6 GHz, i.e., 1 GHz, 4 GHz, 12 GHz, and 24 GHz. By comparing results from multi-frequency measurements, the frequency-dependent characteristics can be analyzed and modeled. Another essential concern in AG channel modeling is the impact of the UAV altitude on the propagation channel. Numerous studies in the physical layer have shown that the height of UAV has a significant impact on the signal transmission [6]. For instance, the authors conducted AG channel measurements over cellular networks, where the height of drone ranges from 1.5 m to 120 m [7]. The results show that as the height rises, the path loss exponent (PLE) decreases from 3.7 to 2.0, which suggests that the scattering environment gradually becomes simple with the height. Thus, it is critical to present a height-dependent channel model for providing a reference design for the upper layers. Moreover, UAVs can be operated at different altitudes, which brings significant challenges to channel modeling. Therefore, in this paper, we also highlight vertical flights of the UAV and aim at analyzing the impact of altitude.

It is known that the popular methods of channel modeling can be classified into three kinds: ray-based deterministic modeling, geometry-based stochastic modeling, and measurement-based empirical modeling [8]. In this paper, empirical modeling is adopted based on channel measurements at multiple frequency bands. Thus, we briefly review the measurement-based AG channel modeling work herein. In our prior work, AG channel measurements are conducted in semiurban environments at L-band and C-band [9], [10], and the ray-tracing simulations are used to validate the multipath propagation [11]. Shi *et al.* conducted measurements for drone-to-ground channels in the line-of-sight (LOS) and non-LOS (NLOS) cases at 900 MHz, 1800 MHz, and 5 GHz, in which log-distance path loss model was used to predict the fading behavior [12]. The four independent altitudes (0 m, 10 m, 20 m, and 30 m) of the UAV were used for comparing the characterizations of AG channel. However, the database is insufficient to propose a completed model with four discrete altitudes. In addition, Amorim *et al.* proposed a height-dependent log-distance $\alpha - \beta - \gamma$ path loss model by means of the fitting of measurement data at 1.5 m, 15 m, 30 m, 60 m and 120 m [13]. Since authors focus on the AG channel over cellular networks, the single long-term evolution (LTE) band–800 MHz was used in measurements, and the impact of different frequency bands remains unknown.

There are scarce studies that jointly investigate the impacts of the vertical altitude and the multiple frequency bands. Thus, the scope of this paper is to measure and analyze low-altitude multi-frequency AG propagation channels. Our main contributions can be summarized as follows.

- We conduct AG channel measurements for UAV vertical flights at different frequencies at almost continuous altitudes in 0-24 m. The large-scale and small-scale channel parameters such as path loss, shadow fading (SF), small-scale fading, level crossing rate (LCR), and average fade duration (AFD), are extracted.
- The PLEs and height impact factor, compatible with the 3GPP three-dimensional (3D) path loss model, are extracted. Compared to the default 3GPP values, we show that our results are better able to predict the path loss of the AG channel.
- A novel autocorrelation function (ACF) model of shadowing is proposed. Also, the proposed model is effective both in LOS and NLOS cases. For the best fit of small-scale fading, the theoretical probability distribution is found based on the criterion of minimum root mean square error (RMSE).
- In addition to quantitative analysis of the path loss, shadowing and small-scale fading, two essential parameters in the second-order statistical characterizations of fading, the AFD and LCR, are analyzed to investigate the detailed behavior of small-scale fading.

The remainder of this paper is organized as follows. In Section II, we introduce AG channel measurements, including the measurement system and setup, and data acquisition. Section III presents the large-scale fading characteristics and the corresponding analysis. An improved path loss model and a novel autocorrelation model of shadowing are proposed, respectively. Section IV focuses on small-scale fading characteristics, where the fading behavior is statistically analyzed, and its theoretical probability distribution is discussed. Moreover, the second-order fading characteristics are qualitatively analyzed. Conclusions are drawn in Section V.

II. AG CHANNEL MEASUREMENTS

In this section, AG channel measurements are presented, where the measurement system and setup are first introduced. Then, data acquisition and processing are described, which gives an illustration for the extractions of the large-scale and small-scale parameters from the received data. It is noted that the narrowband measurements were conducted on the campus of the Technical University of Madrid, which is a semi-urban scenario according to the height and the density of buildings in this environment.

A. MEASUREMENT SYSTEM

The measurement system is composed of DJI N3 six-rotor drone, a test transmitter (Tx), signal analyzer, laptop, and antennas. Fig. 1 depicts the detailed integration of Tx unit in the aircraft together with the battery, telemetry unit, Global Positioning System (GPS) module, and Tx antenna. The UAV belongs to the type of 'small' UAVs with a weight of 4.7 kg

and can be operated in low altitudes. The battery and the telemetry give support on the power and control for flights, respectively. The GPS module can provide an accurate altitude.

At the Tx end, the UAV-integrated test Tx is equipped with a Rugged Surface Mount-Wideband High Frequency (RM-WHF) antenna with 3 dBi gain for 4 GHz and three $\lambda/4$ monopole antennas with 5.19 dBi gain for 1 GHz, 12 GHz, and 24 GHz, respectively. The transmitted signal is a continuous wave (CW) signal with the power of 30 dBm. The ground unit at the receiver (Rx) end is composed of a spectrum analyzer with a $\lambda/4$ monopole antenna with 5.19 dBi gain for 1 GHz, a RM-WHF antenna for 4 GHz and a R&S HL050 antenna with 8 dBi gain for 12 GHz and 24 GHz. The Rx uses a 100 kHz channel filter and its sensitivity of is -120 dBm. Therefore, the link margin is 150 dB, which can provide enough dynamic range to carry out measurements in both the LOS and the NLOS case.

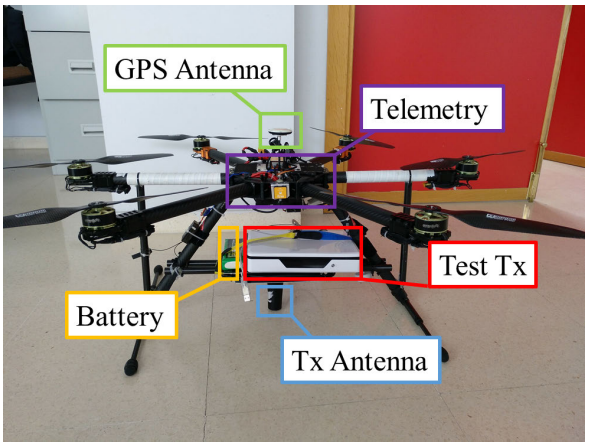

FIGURE 1. Details of the experimental measurement UAV system.

B. MEASUREMENT SETUP

The detailed setup of the measurements is drawn in Fig. 2. The altitude of the UAV h_{U} changes from 0-24 m and the height of GS h_{G} is set to 25 m, which corresponds to the parameters in the 3GPP TR 38.901 urban macro (UMa) scenario setting where BSs are set to 25 m and 1.5-22.5 m for the user equipment (UE) [14], which allows us to compare our results with the standard model. Moreover, there is a building obstructing the LOS path between the Tx and the Rx at certain altitudes. According to the environment geometry, the propagation link is NLOS when the height of UAV is below 11 m, and changes to LOS when higher than 11 m. The measurement environment provides the benefit to measure both LOS and NLOS cases of AG channels. To reduce the error, we carried out five round-trip measurements for each frequency, and the final received power was obtained by averaging the raw data. In the flight, the speed of UAV remains relatively constant at 1 m/s.

All antennas are configured with the vertical polarization, and the radiation patterns of both ends are approximately omnidirectional. In channel measurements, the antenna elevation angles used for measurements is $-30°$ to $30°$ and $-120°$ to $-60°$ for Rx and Tx, respectively. Moreover, as shown in Fig. 2, the horizontal distance is $D = 350$ m, and the height of UAV h_{U} goes from 0 to 24 m, the elevation angle $\theta = \arctan(\frac{h_{\mathrm{G}}-h_{\mathrm{U}}}{D})$ between Tx and Rx is tiny with a range of 0°-4°. Such a small range of θ can ensure that the antennas are properly aligned and that the radiation pattern of antenna does not change significantly during the measurements.

FIGURE 2. Measurement environment and setup where the altitude of the UAV-integrated Tx is 0-24 m (round-trip flights) and the Rx height is 25 m.

C. DATA ACQUISITION AND PROCESSING

The raw data was stored for five round-trip measurements for each frequency in 0-24 m. After averaging raw data, the received power for each frequency has 1500 samples because the sampling interval is 0.016 m for 24 m vertical distance. We can obtain the propagation loss by subtracting the received signal power from the transmitted power where antenna gains have also been included in calculations. we divide the total propagation loss into three scales of spatial variation such as small-scale fading, shadowing and path loss, which can be expressed as

$$\Phi = PL + X_{\sigma} + S_{\beta}, \tag{1}$$

where Φ is the total propagation loss and PL is the path loss. X_{σ} represents the shadowing occurring at dozens of wavelengths, which is conventionally modeled as a zero-mean Gaussian process, with a standard deviation of σ. Since variations of the total propagation loss due to path loss and shadowing occur over relatively large distances, this variation is sometimes referred to as large-scale fading. Then, the variation due to the constructive and destructive addition of multipath signal components occurs over very short distances, on the order of the signal wavelength, so these variations are sometimes referred to as small-scale fading or multipath

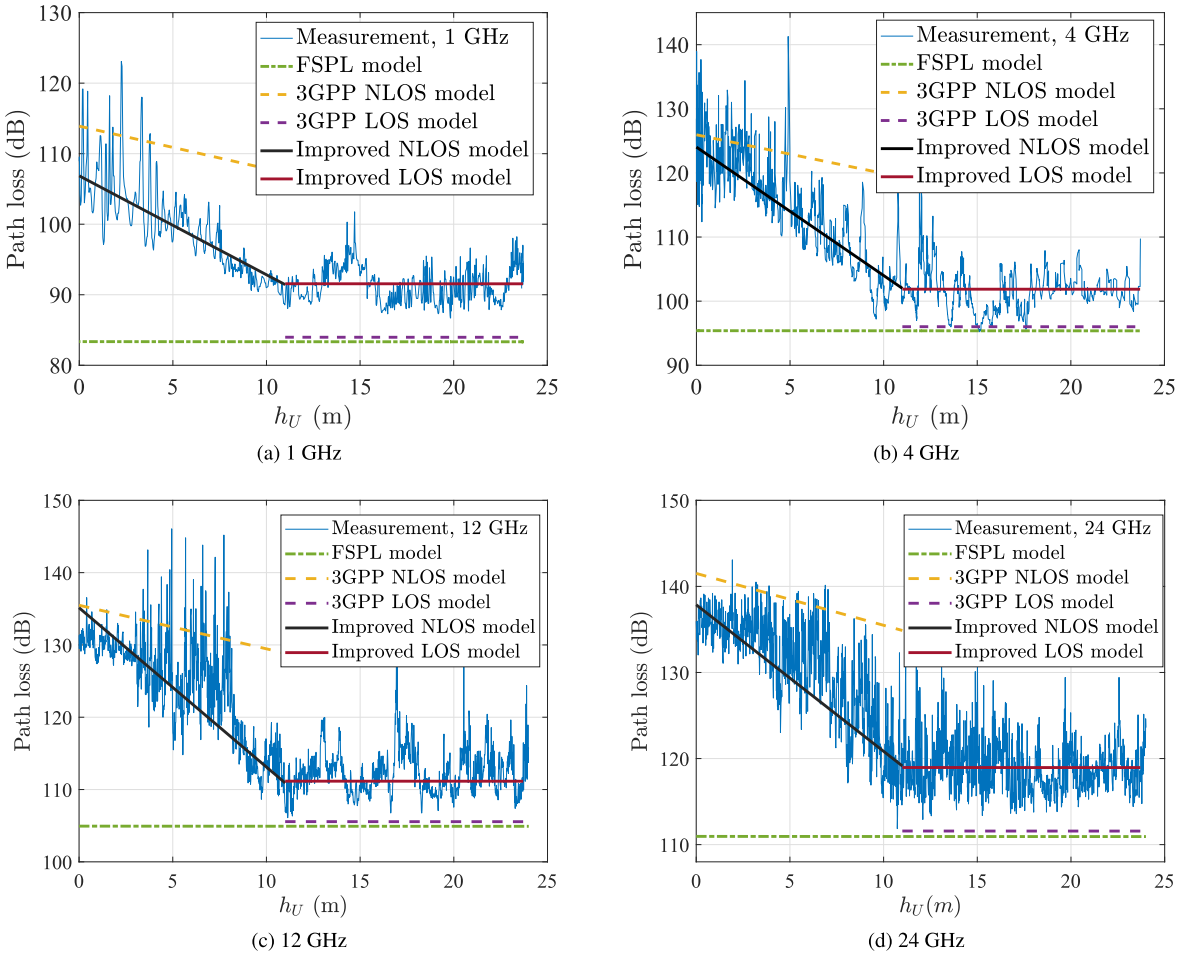

FIGURE 3. Path loss results and modeling with 3GPP model, FSPL and proposed improved 3GPP model: (a) 1 GHz, (b) 4 GHz, (c) 12 GHz, (d) 24 GHz.

fading [15]. The term S_β represents the small-scale fading, which changes rapidly over a few wavelengths.

III. LARGE-SCALE CHARACTERISTICS

The large-scale parameters, including path loss, shadowing, and its autocorrelation, are investigated in this section. The large-scale data are pre-processed by averaging the raw data using a 20-wavelength sliding window. Then, the large-scale parameters can be calculated by their definitions. The highlights in this section include the improved path loss model and the proposed autocorrelation model of shadowing.

A. PATH LOSS

In this section, the path loss is extracted from the raw data. Since the scenario and the the heights of transceiver are similar to the 3D path loss model in the UMa scenario of the 3GPP TR. 39.901 channel model, this model is used to fit our measurement results. The model under the LOS case in the UMa scenario can be expressed as

$$PL_{3GPP}^{LOS} = 28 + 10 \cdot n_{LOS} \log_{10}(d_{3D}) + 20 \log_{10}(f). \quad (2)$$

For the NLOS condition, the path loss model is expressed as

$$PL_{3GPP}^{NLOS} = 13.54 + 10 \cdot n_{NLOS} \log_{10}(d_{3D}) + 20 \log_{10}(f) - \rho(h - 0.5), \quad (3)$$

where n_{LOS} and n_{NLOS} are PLEs for LOS and NLOS case, respectively. ρ is the height impact factor used to introduce the influence of the user height. f and d_{3D} are the carrier frequency in GHz and the Tx-Rx link distance in m, respectively. Note that in the 3GPP model, the standard values of n_{LOS}, n_{NLOS}, and ρ are suggested as 2.200, 3.908, and 0.60, respectively. In order to compare our results with the free-space path loss (FSPL) model, we give its formula that is derived from the Friis's transmission law, which is expressed as

$$PL_{FSPL} = 32.4 + 20 \log_{10}(d_{3D}) + 20 \log_{10}(f), \quad (4)$$

where d_{3D} is in km and f is in MHz.

As shown in Fig. 3, the FSPL model has a poor performance to predict the path loss. With the standard values of n_{LOS}, n_{NLOS}, and ρ given in the 3GPP model, the fitting results also exhibits large deviations from the measurement results. By using a least-square (LS) method, a good

TABLE 1. Results of large-scale channel parameters.

f	n_{LOS} (11-24 m)	n_{NLOS} (0-11 m)	ρ (NLOS)	σ_{LOS} (dB)	σ_{NLOS} (dB)
1 GHz	2.498	3.584	1.40	2.50	3.72
4 GHz	2.420	3.788	2.07	3.17	4.16
12 GHz	2.468	3.537	1.73	2.48	3.56
24 GHz	2.491	3.755	1.59	2.75	3.22
Mean value	2.470	3.666	1.70	2.73	3.67
3GPP [14]	2.200	3.908	0.60	4.00	6.00

agreement can be observed between the measurements and the model. The corresponding results of n_{LOS}, n_{NLOS} and ρ for each frequency are listed in Table 1. It is critical to compare our results with existing AG channel measurement. Authors in [9] conducted similar measurements for low-altitudes flights ($\leq$30 m) at L-band and C-band, where the PLEs obtained by the log-distance model range from 2.64 to 3.35, which are similar to our results with PLEs from 2.42 to 3.79. Moreover, authors in [16] carried out AG channel measurements for higher altitudes (171 m-776 m), where the PLEs are 1.70 and 2.00 for C-band and L-band, respectively. These comparisons show that AG channels in low altitudes are more vulnerable to experience larger fading exponents, which can be explained by the relative complex scattering environment from the perspective of physical meaning.

Overall, the values of PLE between our LS results and the 3GPP standard values are similar. However, the height impact factors of our fitting are much larger than the 3GPP value. This indicates that the 3GPP model values, which are designed for ground-based users, are not appropriate for AG channels where height is an important factor. The results in Table 1 show that the average values of n_{LOS}, n_{NLOS}, and ρ are 2.470, 3.666 and 1.70, respectively. It is noted that the factors are mostly environment-related which account for the differences between our results and those in the 3GPP model. It can also be observed that these coefficients do not show any significant change with frequency. It is acknowledged that the larger impact factor suggests the higher correlation between the altitude and path loss. From the perspective of physical meaning, it can be observed that the shadowing factor at 4 GHz is also larger than that in the other three frequencies, which illustrates that more serious shadowing in the NLOS case leads to a higher height impact factor. For future research, more frequencies can be included in the measurements so that the frequency-dependence can be better analyzed.

B. SHADOW FADING AND AUTOCORRELATION

The shadowing fluctuation (in dB) is usually characterized by a zero-mean Gaussian distribution, i.e., $X_\sigma \sim \mathcal{N}(0, \sigma^2)$ where σ models the power fluctuations around the mean path loss caused by shadowing. Note that although there is no shadowing in the LOS case, the SF is generally used to represent the fluctuation around the path loss curve. The results for four frequencies are listed in Table 1. The mean values of σ are 2.73 dB and 3.67 dB for the LOS and NLOS cases, respectively, which are smaller than the suggested values of the 3GPP model where σ is suggested as 4 dB and 6 dB for the LOS and NLOS, respectively. As shown in Fig. 2, the buildings in the environment are sparsely distributed, which leads to slight shadowing. Besides, since some flight altitudes are higher than the mean height of buildings (around 15 m), the shadowing becomes less significant.

The autocorrelation of SF is of interest for power control and base station (or access point) location design. It is defined as the correlation of SF at different locations of the receiver. For a given height resolution Δh, the autocorrelation in the vertical dimension can be expressed as

$$\hat{\rho}_{\text{auto}}(\Delta h) = \frac{E\{X_\sigma(h)X_\sigma(h+\Delta h)\}}{\sigma(h)\sigma(h+\Delta h)}, \tag{5}$$

where $X_\sigma(h)$ is the value of shadow fading in the position with altitude h; $X_\sigma(h+\Delta h)$ is the value of shadow fading in the position with altitude $h+\Delta h$. $\sigma(h)$ and $\sigma(h+\Delta h)$ are the standard deviations of shadow fading, respectively.

Generally, the autocorrelation of SF can be modeled as an exponential decay function. The single exponentially decaying model (SEDM) was proposed by Gudmundson [17], which is expressed as

$$\hat{\rho}_{\text{auto}}(\Delta h) = \exp\left(-\frac{\Delta h}{h_{\text{cor}}}\right), \tag{6}$$

where h_{cor} represents the decorrelation distance mainly defined as $1/e$ or 0.5 [18]. Note that in a land mobile system, the autocorrelation is modeled as a function of the distance d. Since we focus on the vertical flights in this paper, the corresponding variables are related to the UAV altitude h_{U}.

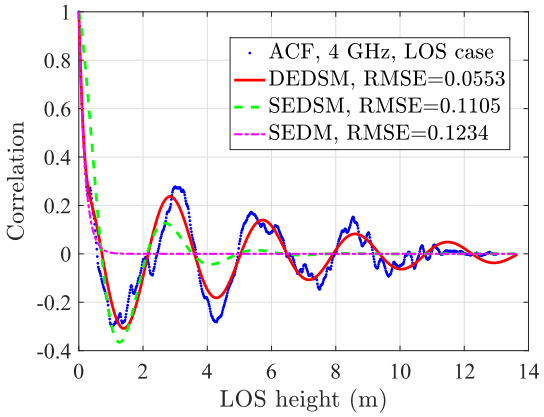

FIGURE 4. Example plot of ACF for SF:LOS case at 4 GHz.

For different propagation links, the SEDM can not describe autocorrelation characteristics well. Thus, the sinusoidal function is introduced into the exponential model. The single exponentially decaying sinusoid model (SEDSM) can be expressed as [19]

$$\hat{\rho}_{\text{auto}}(\Delta h) = \exp\left(-\frac{\Delta h}{h_1}\right)\left[\cos\left(\frac{\Delta h}{h_2}\right)\right]. \tag{7}$$

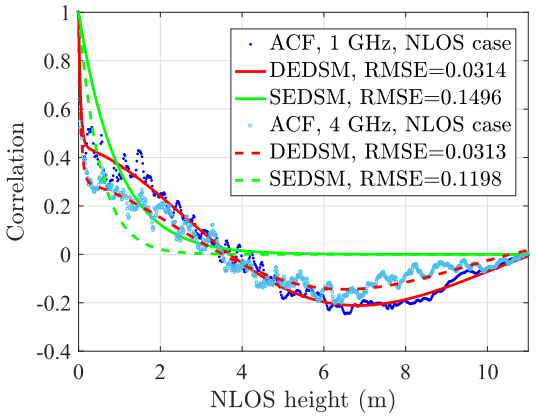

FIGURE 5. Example plot of ACF for SF: NLOS case at 1 GHz and 4 GHz.

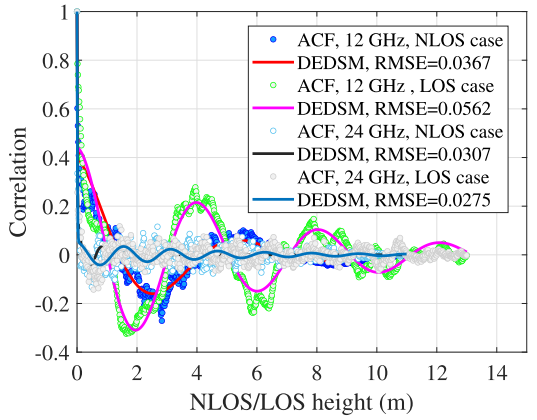

FIGURE 6. Fitting of proposed model for ACF at 12 GHz and 24 GHz.

Another model for the autocorrelation function that can be used in a small UMa scenario is the double exponentially decay model (DEDM) [20], defined as

$$\hat{\rho}_{\text{auto}}(\Delta h) = a \exp\left(-\frac{\Delta h}{h_1}\right) + (1-a)\exp\left(-\frac{\Delta h}{h_2}\right). \quad (8)$$

Due to considerable error existing when fitting with the above models, we propose the double exponentially decaying sinusoid model (DEDSM) by combining the SEDSM and DEDM, which is expressed as

$$\hat{\rho}_{\text{auto}}(\Delta h) = a \exp\left(-\frac{\Delta h}{h_1}\right)\cos\left(\frac{\Delta h}{h_2}\right) + (1-a)\exp\left(-\frac{\Delta h}{h_3}\right)\cos\left(\frac{\Delta h}{h_4}\right), \quad (9)$$

where a, h_1, h_2, h_3, h_4 are determined by fitting results. It is important to illustrate how we proposed the new model. We can find that the existing models of the autocorrelation function for the shadowing are based on two basis functions: the sinusoidal function and the exponential decay function, which are the most popular functions to describe the autocorrelation. We also can find that the exponential decay function must exist in models since it is used to express the decay. While the sinusoidal function is generally used to express the ups and downs of the autocorrelation curve and cannot be used alone. Thus, the available combinations of them include the SEDM, SEDSM, DEDM, and our proposed model-DEDSM. When processing the results, we have tried to use the first three models to fit the measurements, however, the degree of the fitting is low, which explains why we proposed a new model to expect a good fitting.

Figure 4 shows a comparison of the SEDM, SEDSM, and our proposed DEDSM for LOS case at 4 GHz. It can be seen that the RMSE of our model is the lowest, indicating that our proposed model has a better description of the ACF of SF. As shown in Fig. 5, we compare our model with SEDSM at 1 GHz and 4 GHz for the NLOS case. The results show that our model also can fit the curve better than SEDSM. Furthermore, the fitting results for 12 GHz and 24 GHz with the LOS and NLOS cases are plotted in Fig. 6, which also shows good performances with our proposed model. Overall, the proposed model is effective both in LOS and NLOS cases. Thus, we use the model to describe the ACF for all frequencies, and the fitted parameters are summarized in Table 2. The results can be used for the design and simulation of the physical layer.

TABLE 2. Results of the proposed DEDSM for shadowing autocorrelation.

f	Link	a	h_1	h_2	h_3	h_4
1 GHz	LOS	0.36	4.787	0.516	0.207	111.4
	NLOS	0.59	0.055	84.98	9.372	2.388
4 GHz	LOS	0.30	9.259	2.243	0.052	120.9
	NLOS	0.33	0.056	29.41	8.264	2.241
12 GHz	LOS	0.27	6.716	0.621	0.136	33.11
	NLOS	0.48	0.016	195.8	1.709	1.367
24 GHz	LOS	0.39	1.269	0.477	0.265	225.3
	NLOS	0.49	0.012	9.285	2.927	2.069

TABLE 3. Statistical results of small-scale fading.

f	Link	Max. fading value(dB)	1%(dB)	50%(dB)	Fading depth(dB)
1 GHz	LOS	5.932	-2.909	-0.104	2.805
	NLOS	17.08	-7.021	-0.299	6.722
4 GHz	LOS	5.360	-1.878	0.043	1.921
	NLOS	11.25	-5.049	-0.231	4.818
12 GHz	LOS	5.007	-2.063	0.007	2.056
	NLOS	14.72	-6.373	-0.072	6.301
24 GHz	LOS	12.72	-4.913	-0.352	4.561
	NLOS	14.18	-6.927	-0.167	6.760

IV. SMALL-SCALE CHARACTERISTICS

The small-scale fading characteristics are analyzed in this section. The effects of large-scale fading are removed by averaging with a 20-wavelength sliding window. By taking large-scale data away from the raw data, the small-scale fading can be obtained. Thus, in this section, the small-scale fading is statistically analyzed, and the fading depth can be calculated. It is highlighted that the best fit can be found based on the criterion of the minimum RMSE. Besides, we analyze the second-order statistical characteristics of fading according to the definitions of AFD and LCR.

A. SMALL-SCALE FADING AND DEPTH

The results of small-scale fading versus the UAV altitude h_U are shown in Fig. 7(a). Overall, the fading in the NLOS case is more severe than in the LOS case. In Fig. 7(b), we plot the cumulative probability distribution functions (CDFs) of small-scale fading for different frequencies and propagation links, which can be used to determine the fading depth. The fading depth is defined in terms of the difference in power levels between the 50% and 1% level values for each case [21]. The results are summarized in Table 3. As expected, the fading depth under NLOS case is larger than the LOS case. It also can be observed that the fading depth does not seem to be related to frequency.

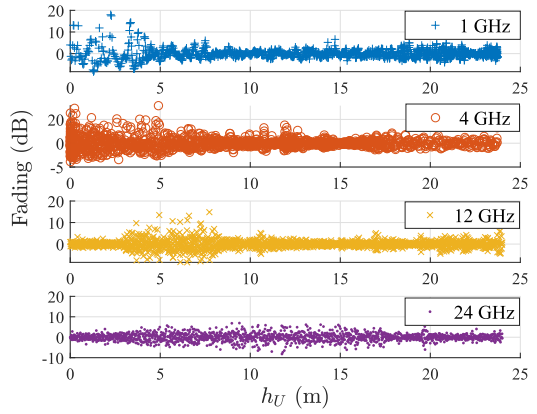

(a) Small-scale fading versus UAV altitude

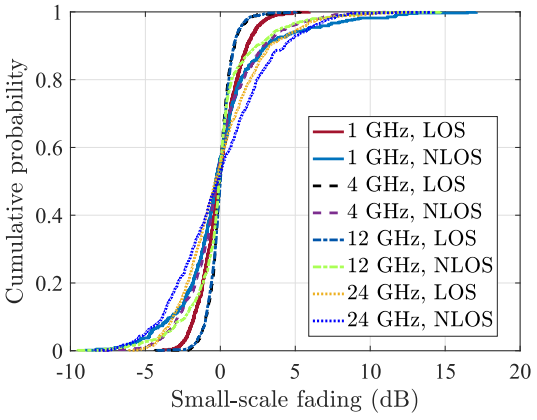

(b) CDFs

FIGURE 7. Small-scale fading: (a) Fading versus UAV altitude, (b) CDFs.

B. BEST FIT DISTRIBUTION OF SMALL-SCALE FADING

It is critical to find the best-fitting theoretical distribution for the amplitude of fading. It is well-known that Nakagami, Rician, Rayleigh, Weibull, and Gaussian distributions are widely used for describing the small-scale fading [22]. It was also shown in [23] that the log-logistic distribution is the best fit for the fading amplitude in a foliage environment. In this paper, we found that the log-logistic distribution is the most suitable distribution to characterize the small-scale fading of AG channel. As shown As an example plot, the probability density function (PDF) of the fade envelope in the LOS case at 12 GHz is shown in Fig. 8. It shows that the log-logistic distribution shows better performance than other popular distributions. We found that the Gaussian distribution with the unity mean and small standard deviation also has a considerable ability to describe the kurtosis of PDF of small-scale fading

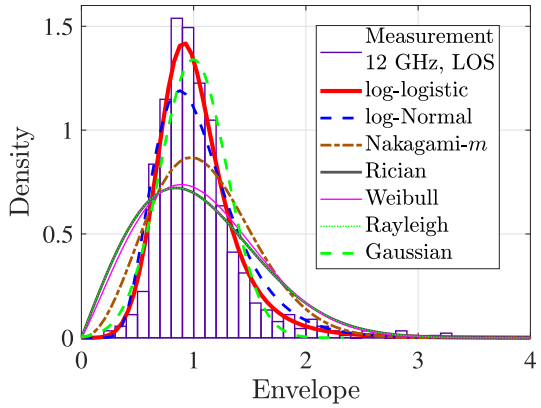

FIGURE 8. PDFs of fade envelope with popular probability distributions fitting.

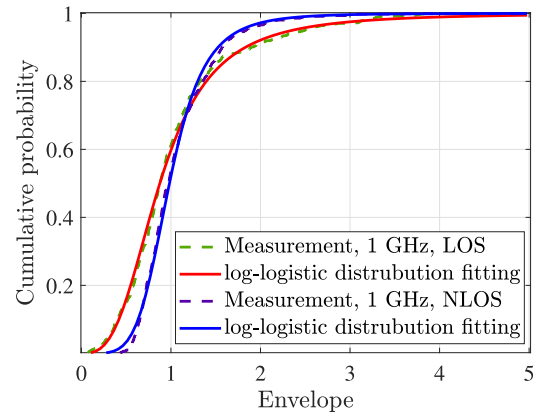

(a) CDFs of fading and log-logistic fitting at 1 GHz

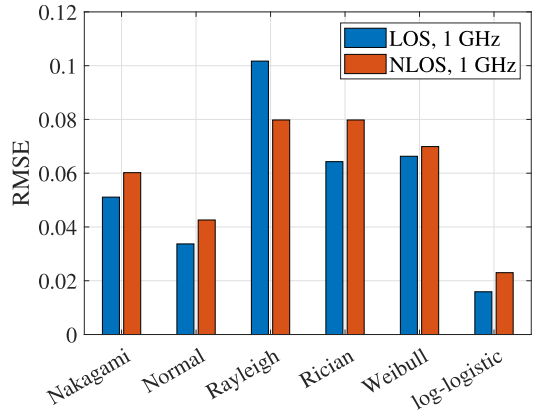

(b) RMSE of fitting for different distributions

FIGURE 9. Best fit of fading: (a) CDFs at 1 GHz, (b) Comparison of RMSE.

at 12 GHz. However, it shows worse performance to describe the skewness of PDF than the log-logistic distribution. Same with the result in [23] for a foliage environment, the log-logistic distribution is found as the best fit, since there are many trees shown in Fig. 2, which may imply that multipath components from trees have strong impacts on deciding the statistical distribution of small-scale fading.

In order to quantitatively show that the log-logistic distribution is the best fit among the candidate distributions, the RMSE is calculated for the LOS and NLOS cases at 1 GHz. As shown in Fig. 9(b), the log-logistic distribution has minimum RMSE in both LOS and NLOS conditions. Moreover, Fig. 9(a) shows a good agreement between the log-logistic distribution and the measurement result. For quantification, we introduce the CDF of log-logistic distribution, which can be expressed as

$$F(x, \alpha, \beta) = \frac{1}{1 + (x/\alpha)^{-\beta}}, \tag{10}$$

where α is a scale parameter and close to 1 in our fitting in both LOS and NLOS at four frequencies, which is due to the mean value close to 0 dB on the dB scale. While β is a shape parameter that determines the steepness of the distribution curve. In our fitting, the values of β for the LOS and NLOS case are (1.41, 1.74, 1.83, 1.89) and (1.12, 1.38, 1.42, 1.65) at (1, 4, 12, 24) GHz, respectively. The results show that the values increase with the frequency, which indicates that the AG channel in the high frequency is more vulnerable to experience severe fading.

C. SECOND-ORDER STATISTICAL CHARACTERISTICS

The second-order statistics of the propagation channel are provided in terms of two major parameters: LCR and AFD, which can be obtained from the received signal strength variations at a single frequency as a function of time or distance [24], [25]. In this paper, due to vertical flights of UAV, the LCR is modeled as a function of the vertical distance. Moreover, the speed of the UAV is almost constant at 1 m/s, the AFD can also be modeled as a function of the vertical distance because of $t = h_U/v$ where v is the velocity, and t is time. According to the definitions, the LCR is the number of the times at which the specified level is crossed in the positive-going direction (down to up), whereas the AFD is the duration (or distance) that the signal remains below the level [24]. For example, for a given threshold of -0.5 dB, Fig. 10 shows an example of LCR and AFD calculation. The circles indicate each time the threshold is crossed, and the double arrow represent represent the vertical distance during which the signal remains below the threshold. If we consider a window with the length of λ, the LCR is 0.15 (3/20) and the AFD is $(d_1 + d_2 + d_3)/(20 \times 3)$ where the crossing number that is used to average the fading. In the paper, the LCR values indicate the crossing times per window length of λ, and the AFD is also expressed in terms of the window length.

According to the previous definitions, we calculate the LCR and AFD for all frequencies in LOS and NLOS cases.

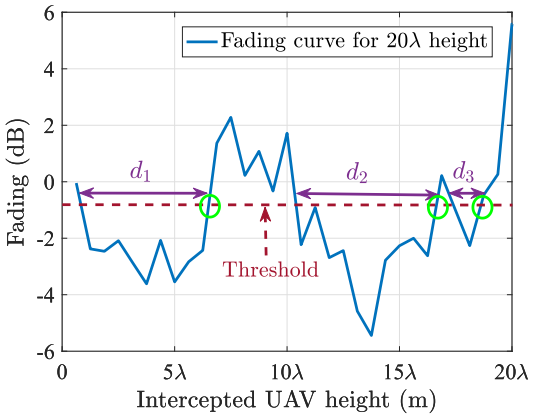

FIGURE 10. Example plot of the LCR and AFD calculations from fading curve.

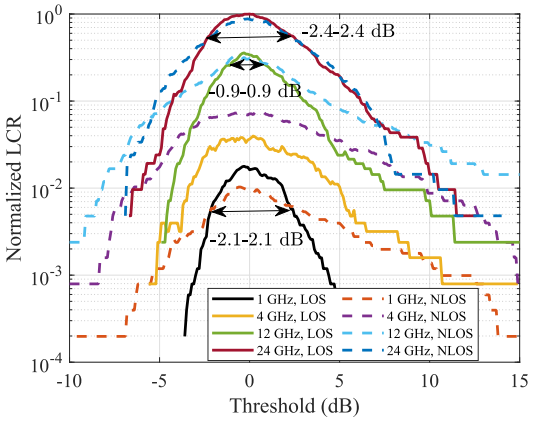

FIGURE 11. Second-order statistical characteristics of fading: LCR.

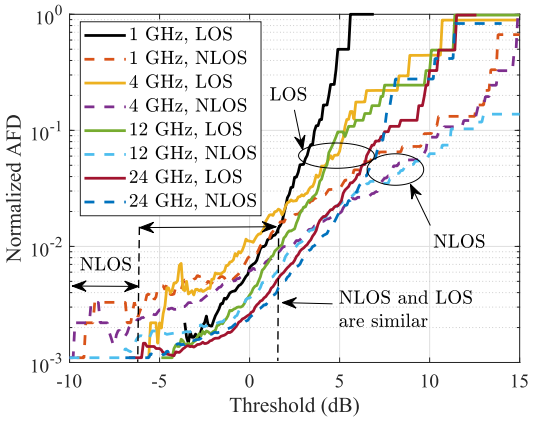

FIGURE 12. Second-order statistical characteristics of fading: AFD.

Note that the LCR and AFD have been normalized for the convenient observation. Generally, as shown in Fig. 11, the LCRs under the NLOS conditions are basically larger than the LOS condition, which means the fading is more variable for the NLOS than for the LOS. However, for a small range of thresholds, the LCRs in the LOS conditions are larger than the NLOS, such as $-2.4-2.4$ dB for 24 GHz, $-0.9-0.9$ dB

for 12 GHz and −2.1−2.1 dB for 1 GHz, which illustrates that the serious fading under the LOS mostly concentrate on a low level. In addition, the frequency-dependence of fading can be found in Fig. 11 where the results show that the high frequency leads to larger fading, which can correspond to Fig. 3 where the curves gradually become more variable from (a) to (d). For the AFD shown in Fig. 12, it can be seen that the larger LCR leads to the smaller AFD since the AFD is divided by the LCR in the calculations. The AFDs in the LOS condition reduce to 0 for all frequencies when the threshold is smaller than −7 dB, which also means the larger fading in the NLOS condition. Overall, the larger LCR and shorter AFD show the more serious fading of radio channels.

V. CONCLUSION

In this paper, the multi-frequency AG propagation channels are investigated for low-altitude UAV vertical flights. The essential large-scale and small-scale channel parameters, including path loss, shadowing, autocorrelation, and small-scale fading characteristics, are comprehensively analyzed and modeled. For the large-scale parameters of AG channels, the mean PLEs are 2.470 and 3.666 for LOS and NLOS case, respectively, which are slightly different from the 3GPP parameters (i.e., 2.200 and 3.908 for LOS and NLOS case). Moreover, the height impact factor for the NLOS condition is found around the average value of 1.70, whereas this parameter is fixed at 0.6 in the 3GPP model. For the shadowing, combining the double exponential decaying model and sinusoidal function, a novel autocorrelation model is proposed and has a better performance than traditional models. Also, the results show that the proposed model can be used both in LOS and NLOS cases. For small-scale characteristics, the fading depth is statistically analyzed, and the results show a weak correlation with the frequency. Through comparisons with the popular distributions using the rule of minimum RMSE, the best fit of small-scale fading is suggested as the log-logistic distribution. Finally, two essential parameters in the second-order statistical characteristics, i.e., LCR and AFD, are extracted according to their definitions. The results of AFD and LCR show that the AG channel under NLOS case experiences more serious fading than the LOS case. The results of this work can be applied to the design and optimization of UAV-based wireless communication systems.

REFERENCES

[1] H. Kim and J. Ben-Othman, "A collision-free surveillance system using smart UAVs in multi domain IoT," *IEEE Commun. Lett.*, vol. 22, no. 12, pp. 2587–2590, Dec. 2018.

[2] Y. Zeng, R. Zhang, and T. J. Lim, "Throughput maximization for UAV-enabled mobile relaying systems," *IEEE Trans. Commun.*, vol. 64, no. 12, pp. 4983–4996, Dec. 2016.

[3] K. Guan, Z. Zhong, J. I. Alonso, and C. Briso-Rodriguez, "Measurement of distributed antenna systems at 2.4 GHz in a realistic subway tunnel environment," *IEEE Trans. Veh. Technol.*, vol. 61, no. 2, pp. 834–837, Feb. 2012.

[4] *Characteristics of Unmanned Aircraft Systems and Spectrum Requirements to Support Their Safe Operation in Non-Segregated Airspace*, document M.2171, ITU-R, 2010.

[5] J. Liu, Y. Shi, Z. M. Fadlullah, and N. Kato, "Space-air-ground integrated network: A survey," *IEEE Commun. Surveys Tuts.*, vol. 20, no. 4, pp. 2714–2741, 4th Quart., 2018.

[6] M. M. Azari, F. Rosas, K. Chen, and S. Pollin, "Optimal UAV positioning for terrestrial-aerial communication in presence of fading," in *Proc. IEEE Global Commun. Conf. (GLOBECOM)*, Washington, DC, USA, Dec. 2016, pp. 1–7.

[7] R. Amorim, H. Nguyen, P. Mogensen, I. Z. Kovács, J. Wigard, and T. B. Sørensen, "Radio channel modeling for UAV communication over cellular networks," *IEEE Wireless Commun. Lett.*, vol. 6, no. 4, pp. 514–517, Aug. 2017.

[8] A. A. Khuwaja, Y. Chen, N. Zhao, M.-S. Alouini, and P. Dobbins, "A survey of channel modeling for UAV communications," *IEEE Commun. Surveys Tuts.*, vol. 20, no. 4, pp. 2804–2821, 4th Quart., 2018.

[9] Z. Qiu, X. Chu, C. Calvo-Ramirez, C. Briso, and X. F. Yin, "Low altitude UAV air-to-ground channel measurement and modeling in semi-urban environments," *Wireless Commun. Mobile Comput.*, vol. 2017, Art. no. 1587412, Nov. 2017.

[10] Z. Cui, C. Briso-Rodríguez, K. Guan, C. Calvo-Ramírez, B. Ai, and Z. Zhong, "Measurement-based modeling and analysis of UAV air-ground channels at 1 and 4 GHz," *IEEE Antennas Wireless Propag. Lett.*, vol. 18, no. 9, pp. 1804–1808, Sep. 2019.

[11] C. Calvo-Ramírez, Z. Cui, C. Briso, K. Guan, and D. W. Matolak, "UAV air-ground channel ray tracing simulation validation," in *Proc. IEEE/CIC Int. Conf. Commun. China (ICCC Workshops)*, Beijing, China, Aug. 2018, pp. 122–125.

[12] Y. Shi, R. Enami, J. Wensowitch, and J. Camp, "Measurement-based characterization of LOS and NLOS drone-to-ground channels," in *Proc. IEEE Wireless Commun. Net. Conf. (WCNC)*, Barcelona, Spain, Apr. 2018, pp. 1–6.

[13] R. Amorim, P. Mogensen, T. Sorensen, I. Z. Kovacs, and J. Wigard, "Pathloss measurements and modeling for UAVs connected to cellular networks," in *Proc. IEEE 85th Veh. Tech. Conf. (VTC Spring)*, Sydney, NSW, Australia, Jun. 2017, pp. 1–6.

[14] *Study on Channel Model for Frequencies From 0.5 to 100 GHz*, document TR 38.901 V14.1.1 Release 14, 3GPP, Aug. 2017.

[15] A. Goldsmith, *Wireless Communications*. Cambridge, U.K.: Cambridge Univ. Press, 2005.

[16] D. W. Matolak and R. Sun, "Air-ground channel characterization for unmanned aircraft systems—Part III: The suburban and near-urban environments," *IEEE Trans. Veh. Technol.*, vol. 66, no. 8, pp. 6607–6618, Aug. 2017.

[17] M. Gudmundson, "Correlation model for shadow fading in mobile radio systems," *Electron. Lett.*, vol. 27, no. 23, pp. 2145–2146, Nov. 1991.

[18] K. Guan, B. Ai, Z. Zhong, C. F. López, L. Zhang, C. Briso-Rodríguez, A. Hrovat, B. Zhang, R. He, and T. Tang, "Measurements and analysis of large-scale fading characteristics in curved subway tunnels at 920 MHz, 2400 MHz, and 5705 MHz," *IEEE Trans. Intell. Transp. Syst.*, vol. 16, no. 5, pp. 2393–2405, Oct. 2015.

[19] Y. Zhang, J. Zhang, D. Dong, X. Nie, G. Liu, and P. Zhang, "A novel spatial autocorrelation model of shadow fading in urban macro environments," in *Proc. IEEE Global Telecommun. Conf.*, New Orleans, LO, USA, Nov./Dec. 2008, pp. 1–5.

[20] A. Algans, K. I. Pedersen, and P. E. Mogensen, "Experimental analysis of the joint statistical properties of azimuth spread, delay spread, and shadow fading," *IEEE J. Sel. Areas Commun.*, vol. 20, no. 3, pp. 523–531, Apr. 2002.

[21] S. Kozono, "Received signal-level characteristics in a wide-band mobile radio channel," *IEEE Trans. Veh. Technol.*, vol. 43, no. 3, pp. 480–486, Aug. 1994.

[22] R. Chen, T. Shi, X. Lv, and Q. Wang, "Small-scale fading characterization for railway wireless channels," in *Proc. IEEE Int. Symp. Antennas Propag. (APSURSI)*, Fajardo, Puerto Rico, Jun./Jul. 2016, pp. 1701–1702.

[23] J. Liang and Q. Liang, "Outdoor propagation channel modeling in foliage environment," *IEEE Trans. Veh. Technol.*, vol. 59, no. 5, pp. 2243–2252, Jun. 2010.

[24] C. Li, K. Yang, J. Yu, F. Li, Y. Shui, F. Chang, and W. Chen, "V2V radio channel performance based on measurements in ramp scenarios at 5.9 GHz," *IEEE Access*, vol. 6, pp. 7503–7514, 2018.

[25] *Multipath Propagation and Parameterization of its Characteristics*, document Rec. ITU-R P.1407-6, ITU-R, Jun. 2017.

ZHUANGZHUANG CUI (Graduate Student Member, IEEE) received the B.E. degree in communications engineering from Beijing Information Science and Technology University, Beijing, China, in 2016. He is currently pursuing the Ph.D. degree with the State Key Laboratory of Rail Traffic Control and Safety, Beijing Jiaotong University, Beijing. He was a Visiting Scholar with North Carolina State University and the Technical University of Madrid. His research interests include UAV-based wireless communications, air-to-ground and air-to-air channel modeling and simulations, and fading behavior of propagation channels.

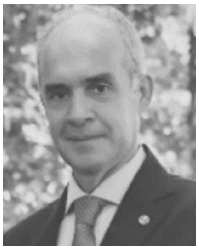

CÉSAR BRISO-RODRÍGUEZ was born in Valladolid, Spain, in 1968. He received the Ph.D. degree in mobile communications from the Universidad Politécnica de Madrid, in 1998. In 2000, he became an Associate Professor with the Technical University of Madrid, where he has been a Permanent Professor, since 2008. He is also an Expert on the design of high-frequency circuits and systems, and in propagation measurements and modeling in complex environments and UAV communication systems. He was a recipient of the National Awards for the Best Ph.D. of the Spanish Association of Telecommunications Engineers.

KE GUAN (Senior Member, IEEE) received the B.E. degree in communications engineering and the Ph.D. degree in communications and information systems from Beijing Jiaotong University, Beijing, China, in 2006 and 2014, respectively.

He is currently an Associate Professor with the State Key Laboratory of Rail Traffic Control and Safety and the School of Electronic and Information Engineering, Beijing Jiaotong University. In 2009, he was a Visiting Scholar with the Universidad Politécnica de Madrid, Spain. From 2011 to 2013, he was a Research Scholar with the Institut fur Nachrichtentechnik (IfN) at Technische Universität Braunschweig, Germany. From September 2013 to January 2014, he was invited to conduct joint research in Universidad Politécnica de Madrid, Spain. He has authored/coauthored two books and one book chapter, more than 200 journal and conference papers, and one patent. His current research interests include measurement and modeling of wireless propagation channels, high-speed railway communications, vehicle-to-x channel characterization, and indoor channel characterization for high-speed short-range systems, including future terahertz communication systems. In 2015, he was awarded the Humboldt Research Fellowship for Postdoctoral Researchers. He was a recipient of the 2014 International Union of Radio Science (URSI) Young Scientist Award. His articles received eight Best Paper Awards, including the IEEE Vehicular Technology Society 2019 Neal Shepherd Memorial Best Propagation Paper Award. He serves as the Publicity Chair for PIMRC 2016, the Publicity Co-Chair for ITST 2018, the Track Co-Chair for EuCNC, the Session Convener for EuCAP 2015–2019, and a TPC Member for many IEEE conferences, such as GLOBECOM, ICC, and VTC. He has been a delegate in 3GPP, and a member of the IC1004 and CA15104 initiatives. He is an Editor of IEEE Access and the *IET Microwave, Antenna and Propagation, and Physical Communication* and a Guest Editor of the IEEE Transactions on Vehicular Technology and the *IEEE Communication Magazine*. He is the Pole Leader of European Railway Research Network of Excellence (EURNEX).

ZHANGDUI ZHONG (Senior Member, IEEE) received the B.E. and master's degrees from Beijing Jiaotong University, Beijing, China, in 1983 and 1988, respectively. He is currently a Professor and the Advisor of Ph.D. candidates with Beijing Jiaotong University. He is also the Director of the School of Computer and Information Technology and the Chief Scientist of the State Key Laboratory of Rail Traffic Control and Safety, Beijing Jiaotong University. He is also the Director of the Innovative Research Team of Ministry of Education, and the Chief Scientist of Ministry of Railways in China. He is an Executive Council Member of the Radio Association of China and the Deputy Director of the Radio Association of Beijing. His research interests include wireless communications for railways, control theory and techniques for railways, and GSM-R systems. His research has been widely used in the railway engineering, such as Qinghai-Xizang railway, Datong-Qinhuangdao Heavy Haul railway, and many high-speed railway lines of China. He has authored/coauthored seven books, five invention patents, and more than 200 scientific research articles in his research areas. He received the Mao Yisheng Scientific Award of China, the Zhan Tianyou Railway Honorary Award of China, and the Top Ten Science/Technology Achievements Award of Chinese Universities.

FRANÇOIS QUITIN (Member, IEEE) received the Ph.D. degree in electrical engineering from the Université Libre de Bruxelles (ULB), Brussels, Belgium, and the Université Catholique de Louvain, Louvain-La-Neuve, Belgium, in 2011. From 2011 to 2013, he was a Postdoctoral Researcher with the University of California at Santa Barbara. From 2013 to 2015, he was a Postdoctoral Research Fellow with Nanyang Technological University, Singapore. He is currently an Assistant Professor with ULB. His research interests include experimental and prototyping aspects in wireless communications, taking advanced theoretical ideas all the way to practice. He received the Alcatel-Lucent Bell Scientific Award, in 2012.